The link between a detached subauroral proton arc and a plasmaspheric plume

M. Spasojević,[1] H. U. Frey,[2] M. F. Thomsen,[3] S. A. Fuselier,[4] S. P. Gary,[3] B. R. Sandel,[5] and U. S. Inan[1]

Received 11 August 2003; revised 10 November 2003; accepted 21 November 2003; published 21 February 2004.

[1] Observations of detached subauroral proton arcs by the FUV instrument on the IMAGE spacecraft have been recently reported and shown to be produced by ring current ions precipitating in the afternoon local time sector during geomagnetically disturbed periods. Data from June 18, 2001 show a direct link between a subauroral proton arc and a global observation of a plasmaspheric plume by the IMAGE EUV instrument. Using a T96 magnetic field model, the proton arc maps to a broad region of enhanced cold plasma density associated with the plume. The link between the proton arc and plume suggests that the precipitation may be due to pitch angle scattering of energetic protons by electromagnetic ion cyclotron (EMIC) waves, which may be preferentially generated within the plume since the presence of cold, dense ions lowers the threshold for the EMIC instability. *INDEX TERMS:* 2716 Magnetospheric Physics: Energetic particles, precipitating; 2768 Magnetospheric Physics: Plasmasphere; 7867 Space Plasma Physics: Wave/particle interactions. **Citation:** Spasojević, M., H. U. Frey, M. F. Thomsen, S. A. Fuselier, S. P. Gary, B. R. Sandel, and U. S. Inan (2004), The link between a detached subauroral proton arc and a plasmaspheric plume, *Geophys. Res. Lett.*, *31*, L04803, doi:10.1029/2003GL018389.

1. Introduction

[2] The first global images of the Earth's proton aurora have been provided by the Far Ultraviolet (FUV) Spectrographic Imager (SI) [*Mende et al.*, 2000] onboard the IMAGE satellite [*Burch*, 2000]. On a number of occasions, arcs of precipitating protons have been observed at latitudes equatorward of and separated from the main proton oval. First reported by *Immel et al.* [2002], these detached subauroral proton arcs appear over several hours of local time in the afternoon sector during geomagnetically disturbed periods and preferentially at times of high solar wind dynamic pressure. Further case studies by *Burch et al.* [2002] show that the subauroral arcs can appear after a change from negative to positive of either the B_z or B_y component of the interplanetary magnetic field (IMF). As a result of either IMF transition, the main proton oval contracts poleward, while the equatorward part of the oval remains at its original latitude. Thus, a separation of several degrees in latitude is created between the new oval position and the presumably preexisting proton arc.

[3] In situ satellite observations from both studies confirm the presence of precipitating protons and an absence of precipitating electrons in these subauroral arcs. While emissions in the main proton oval are due to particles with energies less than 10 keV, the subauroral arcs appear to be produced by precipitating ring current protons with energies in the range of ~10 to 30 keV.

[4] In both studies, the authors noted the tendency for the subauroral arcs to be located in the mid-afternoon sector where, during disturbed periods, plumes of eroded plasmaspheric material can extend sunward from the main plasmasphere. Predicted by numerical modeling for many years [e.g., *Grebowsky*, 1970; *Chen and Grebowsky*, 1974], plasmaspheric plumes were first observed globally by the IMAGE Extreme Ultraviolet (EUV) imager [*Burch et al.*, 2001; *Sandel et al.*, 2001]. The EUV instrument [*Sandel et al.*, 2000] images the Earth's plasmasphere by detecting 30.4-nm radiation resonantly scattered from He^+ ions.

[5] Unfortunately, no EUV plasmaspheric data were available for the detached proton arc events previously reported. However in one of the previously reported cases, the Magnetospheric Plasma Analyzer (MPA) [*Bame et al.*, 1993] onboard the geosynchronously orbiting 1989–046 spacecraft observed enhanced fluxes of low energy plasmaspheric ions in the region where the equatorial extension of the subauroral arc was expected to map [*Burch et al.*, 2001]. Previously, good correspondence has been found between the evolving global structure of the plasmasphere observed by EUV and in situ plasma observations [*Moldwin et al.*, 2003; *Garcia et al.*, 2003; *Spasojević et al.*, 2003].

[6] In this paper, we present results of a case study on June 18, 2001 during which a direct link has been found between a detached subauroral proton arc observed by FUV and a plasmaspheric plume observed globally by EUV.

2. Plasmaspheric Plume Formation

[7] After several days of relatively quiet conditions, a minor geomagnetic storm occurred on June 18, 2001, which was characterized by an ~10 hour period of predominantly southward IMF and relatively high solar wind dynamic pressure (4–12 nT). Signatures of multiple substorms were seen in the AE index, and the Dst index reached a minimum -61 nT. The disturbance onset was initiated by a southward turning of the IMF at ~03:00 UT in conjunction with a

[1]Space, Telecommunications and Radioscience Laboratory, Stanford University, Stanford, California, USA.
[2]Space Science Laboratory, University of California, Berkeley, California, USA.
[3]Los Alamos National Laboratory, Los Alamos, New Mexico, USA.
[4]Lockheed Martin Advanced Technology Center, Palo Alto, California, USA.
[5]Lunar and Planetary Laboratory, University of Arizona, Tucson, Arizona, USA.

0094-8276/04/2003GL018389$05.00

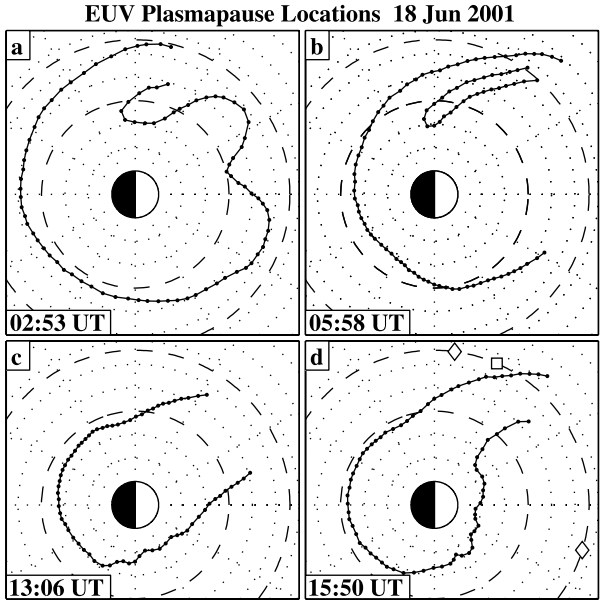

Figure 1. EUV plasmapause locations mapped to the SM equatorial plane. The sun is to the right, concentric dotted circles are spaced 1 R_E apart (r = 4 and 6.6 R_E are dashed circles). In (d), the open square indicates the location of LANL-01a at 15:50 UT, and open diamonds bound the region over which enhanced cold plasma densities were observed in situ (Figure 2a).

steady rise in the solar wind dynamic pressure as measured by the WIND MFI and WIND SWE instruments.

[8] Figure 1 shows the plasmapause locations in the SM equatorial plane as extracted from the EUV global images at four times during the disturbance. Points corresponding to the plasmapause boundary were selected along the sharp brightness gradient on each EUV image, and the points were mapped by finding the field line with the minimum apex along the line of sight to each point (using a tilted dipole field model) and tracing that field line to the equator. (See *Goldstein et al.* [2003] for a discussion of the uncertainty associated with this method.) A plasmapause location is selected only at local times for which a sharp brightness gradient can be reliably identified in the EUV image.

[9] The evolution of the plasmasphere during this disturbed period is morphologically similar to the detailed case studies reported by *Spasojević et al.* [2003]. Just prior to the disturbance onset (Figure 1a), the average equatorial plasmapause location was $r \simeq eq5\ R_E$, yet as is commonly observed by EUV during quiet periods, variations in the plasmapause radius on the order of 1–2 R_E were present [*Sandel et al.*, 2003] and appear as three distinct bulges in the noon to dusk quadrant.

[10] Figure 1b shows the plasmapause locations ~3 hours after disturbance onset. In response to the southward turning of the IMF, inward motion of the plasmapause was observed across the entire nightside. For example at magnetic midnight, the plasmapause moved inward ~1.6 R_E in ~3 hours. In addition, a sunward surge of plasma was observed on the dayside. This motion is particularly evident by the sunward elongation of the azimuthal feature near dusk. The sunward motion effectively moved the plasmapause location inward ~1.1 R_E at 18 MLT, and a narrow low density channel remained between the previously observed azimuthal features.

[11] By the time of the next IMAGE observation period, the IMF B_z had been primarily negative for ~7 hours, and a distinct plasmaspheric plume had formed in the afternoon sector as a result of continued enhanced sunward convection and corotational flows across the dayside. The EUV image at 13:06 UT (Figure 1c) was taken when the satellite was still at a relatively low latitude ($\lambda \simeq eq57°$) so that the plume beyond $r \simeq eq5.5\ R_E$ was outside the field of view.

[12] Just before 15:00 UT, the IMF B_z turned and remained positive for several hours. As a result, the strength of magnetospheric convection decreased, and corotation flows began to dominate the inner magnetosphere. The eastern edge of the plume (Figure 1d) was observed to approximately corotate at r = 4 R_E, but the rate of rotation decreased with increasing radial distance to ~87% of corotation at r = 5 R_E and only ~40% at r = 6 R_E.

[13] During the period of plume formation, the LANL-01a satellite was traversing the dayside, and Figure 2a shows the observed density of cold ions in the range of ~1–130 eV/q from the MPA instrument. Between ~10:00 and 17:00 UT (local time sector between the two open diamonds in Figure 1d), MPA measured enhanced cold ion densities ($n_{ic} > 10\ cm^{-3}$) associated with the initial sunward surge, subsequent plume formation and later plume rotation. In Figure 1d at 15:50 UT, LANL-01a is shown to be located (open square) east of the plume boundary as determined by EUV. However, MPA was measuring cold ion densities of ~15 cm^{-3} associated with the plume but below the effective lower threshold of EUV estimated to be equivalent to a total ion density of 30–50 cm^{-3} [*Goldstein et al.*, 2003; *Moldwin et al.*, 2003].

3. Detached Subauroral Proton Arc

[14] The SI12 channel of the IMAGE FUV instrument produces global images of the proton aurora by detecting Doppler-shifted Lyman-α emission (121.8 nm) from charge-exchanging precipitating protons. An SI12 image

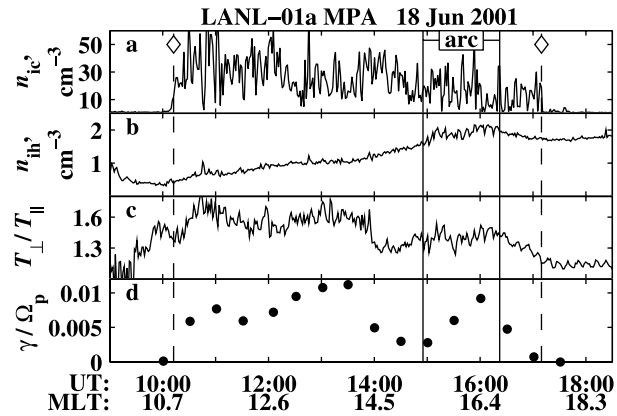

Figure 2. In situ measurements by the MPA instrument on LANL-01a. (a) Cold ion density. (b) Hot ion density. (c) Hot ion temperature anisotropy. (d) Dimensionless growth rate of the proton cyclotron instability calculated from linear Vlasov dispersion theory. The open diamonds correspond to the MLT locations indicated in Figure 1d and the detached proton arc was observed between the solid verical lines.

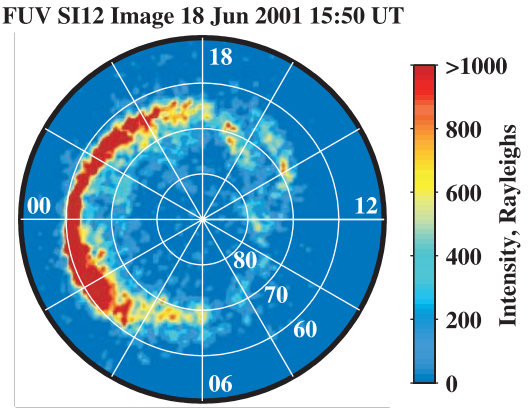

Figure 3. A proton aurora image from FUV SI12 at 15:50 UT mapped onto magnetic latitude and MLT coordinates with the color corresponding to intensity in Rayleighs. Noon is to the right and 60°, 70° and 80° latitude circles are drawn.

from 15:50 UT on June 18, 2001 (the same time as Figure 1d) is shown in Figure 3. A detached subauroral proton arc can be seen in the afternoon sector extending to lower latitudes at later magnetic local times (from $\lambda \simeq 72°$ at ~13 MLT to $\lambda \simeq 64°$ at ~16.5 MLT).

[15] A keogram centered on 16 MLT from the SI12 instrument in Figure 4a shows the temporal development of the detached arc. From ~14:30 to 15:00 UT, bright proton aurora can been seen between ~64°–70° latitude. At ~14:55 UT, a northward and eastward turning of the IMF occurred (Figure 4b), and in response the main proton oval contracted poleward and by 15:50 UT was centered at ~72.5°. However, the equatorward portion of the oval remained at approximately the original latitude, and thus the main oval and the most equatorward arc became separated by several degrees. After ~16:20 UT, the emissions in the detached arc began to fade.

[16] The amount of separation between the main oval and the detached arc increased with increasing magnetic local time. For example, at 15:50 UT at 16 MLT (Figure 4a), there was ~8° of separation between the peak emission in each arc and a relatively clear gap between the two. On the other hand, a similar keogram display for 12 MLT (not shown) showed only ~4° of separation between the peaks, and the two arcs blend together without a clear gap.

[17] Figure 5 shows the EUV plasmapause locations and the equatorward and poleward edges of the detached proton arc at 15:50 UT mapped to the SM equatorial plane using the T96 magnetic field model [*Tsyganenko and Stern*, 1996] and the prevailing solar wind conditions. The detached subauroral proton arc appears to map approximately to the location of the plasmaspheric plume as observed by EUV and MPA. At ~16–17 MLT, the poleward edge of the arc appears to map to higher radial distances than the eastern edge of the plume as observed by EUV, yet measurements by LANL-01a (open square) indicate plume material in this region, but at densities lower than the estimated effective EUV threshold. At earlier local times (13–15 MLT), the arc maps to a region that is outside of the field of view of the EUV instrument, but given the observation that the plume rotated slower at higher radial distances, it is likely that this region also contained enhanced cold plasma densities associated with the plume.

4. Wave-Particle Interactions

[18] The link between the plasmaspheric plume and the detached subauroral proton arc suggests that the precipitation mechanism may be a resonant interaction between ring current protons and electromagnetic ion cyclotron (EMIC) waves which are preferentially generated in the plume region. Although not necessarily the primary loss mechanism of ring current ions, wave-particle interactions may nevertheless play an important role and have been studied extensively (see [*Daglis et al.*, 1999] and references therein).

[19] The sunward transport of ring current ions during disturbed periods produces anisotropic ($T_\perp > T_\parallel$) particle distributions through adiabatic heating. Solar wind compression of the magnetosphere can also increase the ion anisotropy [*Anderson and Hamilton*, 1993]. The anisotropic proton distributions can become unstable to the amplifica-

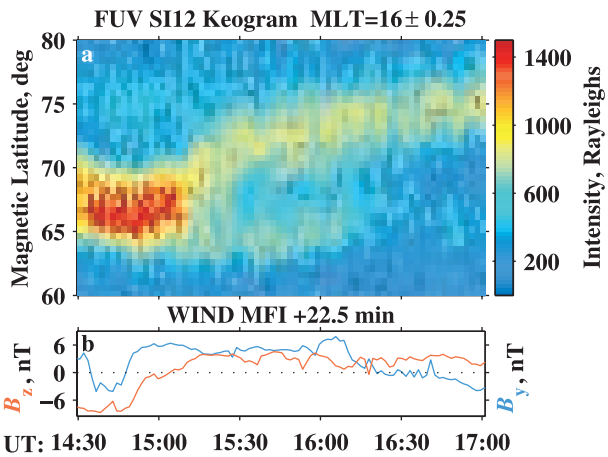

Figure 4. (a) A keogram from the SI12 imager showing the temporal evolution of the proton aurora averaged over a half hour of local time centered on 16 MLT. (b) Solar wind IMF B_z (red) and B_y (blue) from WIND MFI with a 22.5 min transition time correction applied.

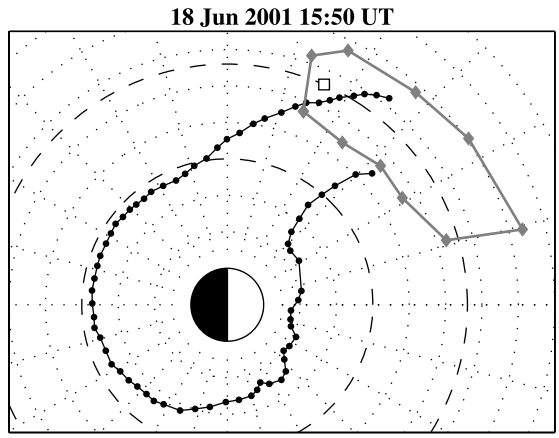

Figure 5. The EUV plasmapause locations (black circles) and the edges of the detached proton arc (gray diamonds) from 15:50 UT are mapped to the SM equatorial plane using the T96 magnetic field model. The open square indicates the location of LANL-01a at this time.

tion of EMIC waves, and specifically the presence of cold dense ions lowers the instability threshold [*Gary et al.*, 1995]. Thus, anisotropic yet stable energetic proton distributions drifting westward from dusk may become unstable when they encounter the enhanced cold plasma densities within the plasmaspheric plume. As a result, EMIC waves would be amplified and can in turn pitch angle scatter the energetic protons into the loss cone.

[20] In addition to the cold ion ($\sim$1–130 eV/q) density, the MPA instrument also measured the hot ion ($\sim$0.13–45 keV/q) density and the hot ion temperature anisotropy ($T_\perp/T_\parallel$) across the dayside and during the period that FUV observed the detached proton arc (Figure 2b–2c). With these plasma observations and the assumption that the background magnetic field was 100 nT, we used linear Vlasov dispersion theory [*Gary et al.*, 1995] to calculate the maximum growth rate of the electromagnetic proton cyclotron instability at half hour intervals, as shown in Figure 2d. After $\sim$16:30 UT, MPA observed a decrease in both the hot ion density and the hot ion anisotropy coincident with the decrease in the intensity of the emissions in the detached proton arc, and growth rate calculations indicate that Alfven-cyclotron mode was stable after 17:00 UT.

5. Conclusions

[21] Although such a relationship was suggested by previous studies [*Immel et al.*, 2002; *Burch et al.*, 2002], we presented here the first observation of a direct link between a detached subauroral proton arc and a globally observed plasmaspheric plume. The geomagnetic disturbance of June 18, 2001, characterized by a prolonged period of southward IMF and high dynamic pressure, led to a buildup of the ring current as measured by the *Dst* index and as observed globally by the IMAGE High Energy Neutral Atom (HENA) imager (not presented here). As suggested by the instability growth rate calculations, proton precipitation may have occurred throughout the disturbance in the region on the dayside filled with plasmaspheric material which over many hours formed the plasmaspheric plume. However, only after the northward (and eastward) turning of the IMF at 14:55 UT, which caused the main proton oval to contract and the plume to rotate toward dusk, was the subauroral proton arc visible and distinct.

[22] **Acknowledgments.** We are grateful to S. M. Petrinec for the T96 mappings to the WIND MFI and SWE teams and the CDA Web for providing the solar wind data. The work at Stanford Univ. was supported by subcontract 03-08482 from the Univ. of Massachusetts Lowell. The work at U.C. Berkeley and the Univ. of Arizona was supported by a subcontract from SwRI, under NASA contract NAS5-96020. Work at Lockheed Martin was funded though a subcontract from U.C. Berkeley. Work at Los Alamos was conducted under the auspices of the U.S. Department of Energy.

References

Anderson, B. J., and D. C. Hamilton (1993), Electromagnetic ion cyclotron waves stimulated by modest Magnetospheric compressions, *J. Geophys. Res.*, *98*, 11,369.

Bame, S., et al. (1993), Magnetospheric plasma analyzer for spacecraft with constrained resources, *Rev. Sci. Instrum.*, *64*, 1026.

Burch, J. L. (2000), IMAGE mission overview, *Space Sci. Rev.*, *91*, 1.

Burch, J. L., D. G. Mitchell, B. R. Sandel, P. C. Brandt, and M. Wuest (2001), Global dynamics of the plasmasphere and ring current during magnetic storms, *Geophys. Res. Lett.*, *28*(6), 1159.

Burch, J. L., et al. (2002), Interplanetary magnetic field control of afternoon-sector detached proton auroral arcs, *J. Geophys. Res.*, *107*(A9), 1251, doi:10.1029/2001JA007554.

Chen, A. J., and J. M. Grebowsky (1974), Plasma tail interpretations of pronounced detached plasma regions measured by Ogo 5, *J. Geophys. Res.*, *79*, 3851.

Daglis, I. A., R. M. Thorne, W. Baumjohann, and S. Orsini (1999), The terrestrial ring current: Origin, formation and decay, *Rev. Geophys.*, *37*, 407.

Garcia, L. N., S. F. Fung, J. L. Green, S. A. Boardsen, B. R. Sandel, and B. W. Reinisch (2003), Observations of the latitudinal structure of plasmaspheric convection plumes by IMAGE-RPI and EUV, *J. Geophys. Res.*, *108*(A8), 1321, doi:10.1029/2002JA009496.

Gary, S. P., M. F. Thomsen, L. Yin, and D. Winske (1995), Electromagnetic proton cyclotron instability: Interactions with magnetospheric protons, *J. Geophys. Res.*, *100*(A11), 21,961.

Goldstein, J., M. Spasojević, P. H. Reiff, B. R. Sandel, W. T. Forrester, D. L. Gallagher, and B. W. Reinisch (2003), Identifying the plasmapause in IMAGE EUV data using IMAGE RPI in situ steep density gradients, *J. Geophys. Res.*, *108*(A4), 1147, doi:10.1029/2002JA009475.

Grebowsky, J. M. (1970), Model study of plasmapause motion, *J. Geophys. Res.*, *75*, 4329.

Immel, T. J., S. B. Mende, H. U. Frey, L. M. Peticolas, C. W. Carlson, J.-C. Gérard, B. Hubert, S. A. Fuselier, and J. L. Burch (2002), Precipitation of auroral protons in detached arc, *Geophys. Res. Lett.*, *29*(11), 1519, doi:10.1029/2001GL013847.

Mende, S. B., et al. (2000), Far Ultraviolet Imaging from the IMAGE Spacecraft. 3. Spectral Imaging of Lyman-α and OI 135.6 nm, *Space Sci. Rev.*, *91*, 287.

Moldwin, M. B., B. R. Sandel, M. F. Thomsen, and R. C. Elphic (2003), Quantifying global plasmaspheric images with in situ observations, *Space Sci. Rev.*, *109*(1–4), 47–61, in press.

Sandel, B. R., et al. (2000), The Extreme Ultraviolet Imager investigation for the IMAGE mission, *Space Sci. Rev.*, *91*, 197.

Sandel, B. R., R. A. King, W. T. Forrester, D. L. Gallagher, A. L. Broadfoot, and C. C. Curtis (2001), Initial Results from the IMAGE Extreme Ultraviolet Imager, *Geophys. Res. Lett.*, *28*(8), 1439.

Sandel, B. R., J. Goldstein, D. L. Gallagher, and M. Spasojević (2003), Extreme Ultraviolet Imager observations of the structure and dynamics of the plasmasphere, *Space Sci. Rev.*, *109*(1–4), 25–46, in press.

Spasojević, M., J. Goldstein, D. L. Carpenter, U. S. Inan, B. R. Sandel, M. B. Moldwin, and B. W. Reinisch (2003), Global response of the plasmasphere to a geomagnetic disturbance, *J. Geophys. Res.*, *108*(A9), 1340, doi:10.1029/2003JA009987.

Tsyganenko, N. A., and D. P. Stern (1996), Modeling the global magnetic field of the large-scale Birkeland current systems, *J. Geophys. Res.*, *101*(A12), 27,187.

M. Spasojević and U. S. Inan, STAR Lab, Stanford University, Stanford, CA 94305-9515, USA. (mssm@nova.stanford.edu)

H. U. Frey, Space Sci Lab., UC Berkeley, CA 94720, USA.

M. F. Thomsen and S. P. Gary, Los Alamos National Lab, MS D466, Los Alamos, NM 87544, USA.

S. A. Fuselier, Lockheed Martin ATC, Palo Alto, CA 94304, USA.

B. R. Sandel, Lunar and Planetary Lab, University of Arizona, Tucson, AZ 85721, USA.